AIAA

A01-34143

AIAA 2001-3377

Solar Thermal Propulsion for an Interstellar Probe

R. W. Lyman, M. E. Ewing, R. S. Krishnan, D. M. Lester
Thiokol Propulsion
Brigham City, UT

R. L. McNutt, Jr.
Applied Physics Laboratory
Johns Hopkins University
Laurel, MD

37th AIAA/ASME/SAE/ASEE Joint Propulsion Conference
July 8-11, 2001
Salt Lake City, Utah

SOLAR THERMAL PROPULSION FOR AN INTERSTELLAR PROBE [*]

Ronald W. Lyman, Mark E. Ewing, Ramesh S. Krishnan, Dean M. Lester,
Thiokol Propulsion
Brigham City, UT

Ralph L. McNutt Jr.
Applied Physics Laboratory
Johns Hopkins University
11100 Johns Hopkins Road
Laurel, MD

ABSTRACT

The conceptual design of an interstellar probe powered by solar thermal propulsion (STP) engines will be described. This spacecraft will use STP engines to perform solar gravity assist with a perihelion of 3 to 4 solar radii to achieve a solar system exit velocity (see Figure 1). Solar thermal propulsion uses the sun's energy to heat a working fluid with low molecular weight, such as hydrogen, to very high temperatures (around 3000 K). The stored thermal energy is then converted to kinetic energy as the working fluid exits a diverging nozzle, resulting in a propulsion system with a high specific impulse (I_{SP}).
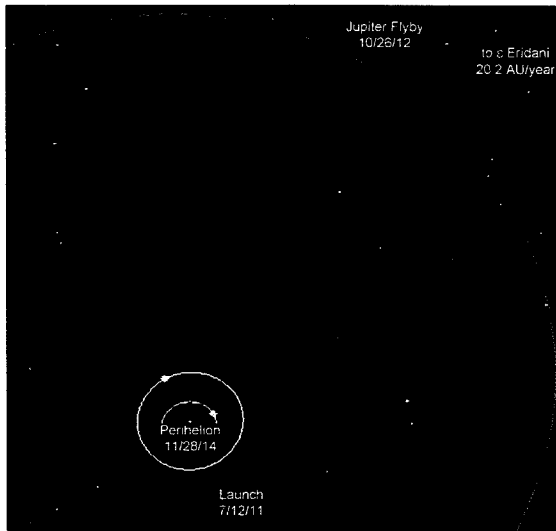
Figure 1. Proposed trajectory for an Interstellar Probe

This paper will evaluate the feasibility of using STP for an interstellar probe. The technology

---

readiness and required system improvements will be identified.

INTRODUCTION

Although traveling to the stars is still beyond the reach of known technology, a probe capable of penetrating the interstellar medium may be within that reach.[1-6] Using a high-thrust, high specific impulse solar thermal propulsion system this probe could potentially achieve an asymptotic escape speed of 20 astronomical units (AU) per year. This mission would utilize a Jupiter flyby and powered perihelion gravity assist.[5, 7-9]

Solar thermal propulsion is an innovative concept that uses the Sun's energy to heat a low-molecular weight fluid such as hydrogen.[10-11] The thermal energy stored in the heated fluid is then converted to kinetic energy by expansion through a diverging nozzle. This results in a high efficiency propulsion system.[12] Spacecraft using STP have been proposed for orbital transfer, interplanetary, and other delta velocity missions.[13]

An interstellar probe using solar thermal propulsion to perform a perihelion maneuver has been proposed.[5, 7-9] The probe itself is small (~50kg). Prior to the solar gravity assist, it is surrounded by a much more massive carrier or cocoon. This cocoon protects the probe and consists primarily of the heat shield and STP system. The thermal model is shown in Figure 2. This diagram shows a vehicle with a
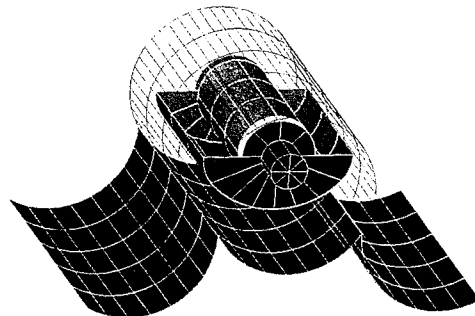
Figure 2. Proposed Interstellar Probe with the pre-maneuver heat shields deployed

deployable exterior heat shield (shown in red) that protects the interstellar probe and propulsion system during its perihelion maneuver. The shield, made of carbon-carbon composite, is opened and oriented toward the sun as the spacecraft approaches perihelion. This hinged device will form a 30° shadow (at 4 solar radii) to thermally protect the probe/carrier assembly.

The center third of the heat shield is the STP engine. This engine is a channeled heat exchanger as shown in Figure 3. During the perihelion maneuver, low-pressure hydrogen (< 1380 kPa) flows through this heat exchanger at 232 g/s for 15 minutes. The channels are sized to achieve a high heat exchanger effectiveness, resulting in a hydrogen exit temperature approaching the theoretical limit for the solar heat source, while minimizing pressure drop of the hydrogen as it passes through the device.
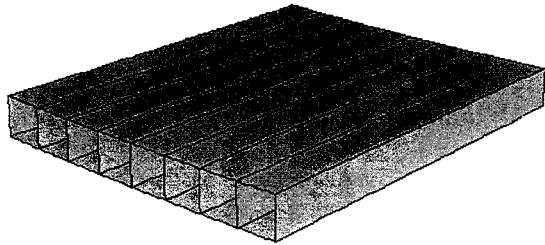
Figure 3. Section of the STP Engine (Channeled heat exchanger)

Once the hydrogen exits the heat exchanger, it is transferred through a plenum to a centroidal nozzle, where the stored thermal energy is converted to thrust. It should be noted that in this feasibility study the designs of the entrance or exit plenums have not been addressed, although a mass allocation has been made.

PROPULSION SYSTEM

The goal for the system is to achieve an escape velocity from the solar system of 20 AU-yr^{-1} (94.8 km-s^{-1}).[7] The mission requires a fast transfer to Jupiter and flyby, where an unpowered gravity assist reduces perihelion of the transfer orbit. In addition, the gravity assist accomplishes a plane change that places the trajectory where a perihelion change in velocity, a delta velocity (ΔV) maneuver, yields the desired solar system escape direction. The ΔV required at perihelion is the difference between the perihelion velocities of the hyperbolic solar-system-escape and elliptical Jupiter-to-perihelion transfer trajectories.

The idea of using a high-I_{SP}, high-thrust maneuver close to the Sun was first identified in 1929

by rocket pioneer Hermann Oberth.[14] Measuring the ΔV in km-sec^{-1} the asymptotic escape speed from the solar system is approximately

$$V_{escape} = (\Delta V)^{1/2} \frac{35.174}{r_p^{1/4}} \frac{km}{s} \; or \; (\Delta V)^{1/2} \frac{7.4142}{r_p^{1/4}} \frac{AU}{yr}$$

where r_p is the distance from the center of Sun in terms of Sun radii (R_S). This equation gives an approximation to the required propulsive maneuver for a given asymptotic speed.

With this relationship the required ΔV is approximately 14.6 km-s^{-1} for a 20 AU-yr^{-1} escape velocity from a 4 R_S perihelion. With a closer approach, 3 R_S perihelion, the required ΔV is reduced to approximately 12.6 km-s^{-1}. However, there are additional factors that must be considered for closer approaches, such as thermal protection methods along with the associated mass increase. As a baseline, the value of $\Delta V = 15$ km-s^{-1} was chosen for the propulsion "target" to enable an asymptotic solar system escape of roughly 20 AU-yr^{-1} from a 4 R_S perihelion.

The relationship between the required ΔV, the system I_{SP} and the mass ratio (MR) or the mass fraction (ζ) is

$$\Delta V = I_{SP} * g_0 \ln\left(\frac{1}{MR}\right)\frac{km}{s} \; or \; I_{SP} * g_0 \ln\left(\frac{1}{1-\zeta}\right)\frac{km}{s}$$

where g_0 is 9.81×10^{-3} km-s^{-1} for a ΔV measured in terms of km-s^{-1}. The mass ratio, MR, is defined as the ratio of the final or dry mass (m_f) to the initial or wet mass (m_i), and the mass fraction, ζ, is the ratio of the propellant mass (m_p) to m_i. The relationship shows that the required ΔV is directly proportional to I_{SP}, and a logarithmic relationship exists with the mass ratio or the mass fraction. To achieve the ΔV maneuver goal of 15 km-s^{-1}, without an unrealizable propellant mass, the I_{SP} must be maximized.

An analysis was made to explore the possible I_{SP} capabilities of potential propellants. (These are propellants in that an external thermal source heats chemically inert material for expulsion in STP instead of providing heat chemically by "burning" a fuel.) These include liquid hydrogen (LH_2), ammonia (NH_3), and methane (CH_4). The baseline propellant selected for reference is LH_2 since it has the potential for the highest I_{SP}. Each candidate was analyzed at various pressure and temperature conditions at the nozzle inlet and allowed to expand through a range of nozzle expansion ratios of 20:1 to 100:1. Pressures of 517 kPa (76 psia) and 1380 kPa (200 psia) were evaluated in combination with a set of temperatures ranging from 1500 K to 3500 K. The feasibility of reaching these temperatures is discussed

later in this report, but it is assumed that at least 2400 K is possible and a 3500 K maximum allows a margin for carbon-carbon material that melts at approximately 3800 K.

The analysis results for H_2 (see Figures 4 and 5) show the highest I_{SP} levels of the three propellants studied. Results of this analyses indicates that at the lower temperatures the pressure does not affect the I_{SP}, while at the upper end of the temperature range, the lower pressure allows for more dissociation of the propellant and thus higher I_{SP} values. The maximum I_{SP} predicted for temperatures of 2400 K, 3000 K, 3300 K and 3500 K are 860 sec, 1037 sec, 1166 sec and 1267 sec, respectively. An observation that can be made from the analysis results is that the nozzle area expansion ratio does not have a large affect on the I_{SP} level at ratios greater 50:1. There is less than a two percent increase in I_{SP} from an expansion ration of 50:1 to 100:1.
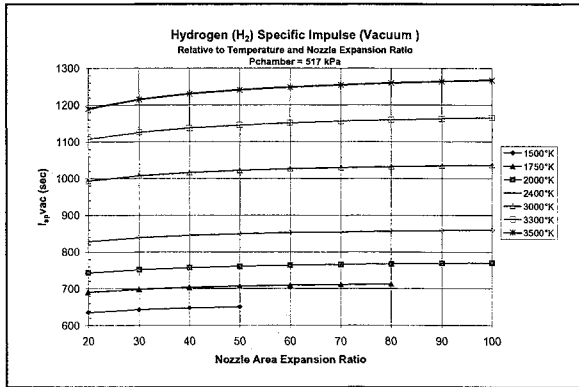
Figure 4. Hydrogen I_{SP} at 517 kPa Initial Pressure
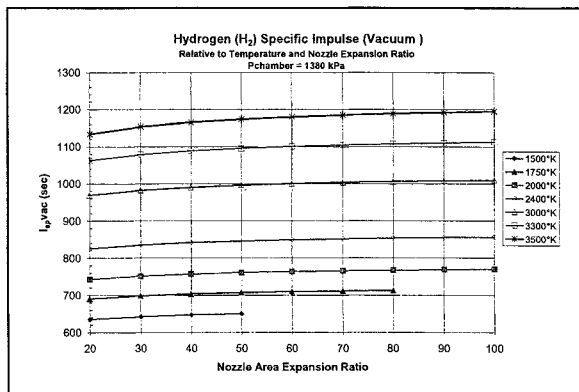
Figure 5. Hydrogen I_{SP} at 1380 kPa Initial

An analysis of methane as a propellant candidate results in the next best I_{SP} levels of the three candidates. This was only evaluated for the four temperatures of 2400 K, 3000 K, 3300 K and

3500 K. The I_{SP} analysis for methane (see Figures 6 and 7) produces similar findings to the hydrogen in terms of higher I_{SP} values at the lower pressure due to more dissociation. The database used for predicting I_{SP}, while accounting for dissociation, is finite and this is apparent in the analysis of CH_4 at 3500 K. The maximum temperature at 517 kPa is limited to 3430 K. The maximum I_{SP} predicted for temperatures of 2400 K, 3000 K, 3300 K and 3430 K are 480 sec, 588 sec, 667 sec and 703 sec, respectively. The expansion ratio has a slightly greater effect with methane in that after an expansion ratio of 70:1, the increase in I_{SP} is less than two percent.
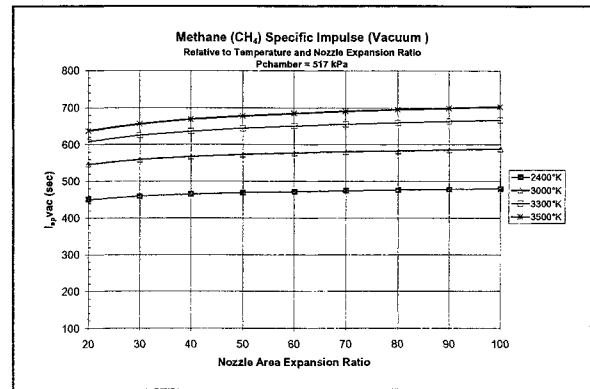
Figure 6. Methane I_{SP} at 517 kPa Initial Pressure
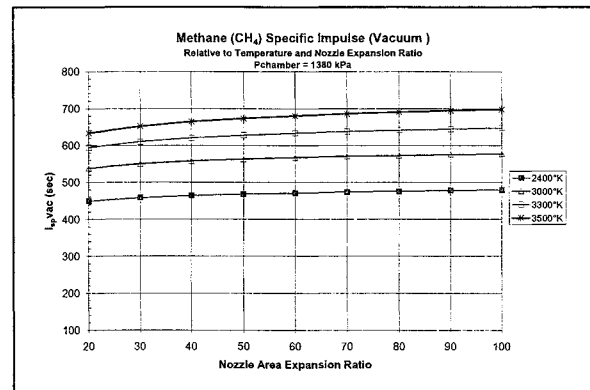
Figure 7. Methane I_{SP} at 1380 kPa Initial Pressure

Ammonia produces the lowest I_{SP} levels of the three propellant candidates. Again the analysis was carried out only at the temperatures of 2400 K, 3000 K, 3300 K and 3500 K. The results of the I_{SP} analysis (see Figures 8 and 9) for ammonia are relatively close to those for methane. Again characteristics are similar to the other two cases in terms of producing higher I_{SP} levels with the lower pressure due to more dissociation. The highest predicted levels of I_{SP} for ammonia are temperatures of 2400 K, 3000 K, 3300 K and 3500 K are 421 sec,

American Institute of Aeronautics and Astronautics

502 sec, 559 sec and 604 sec, respectively. The expansion ratio effects for the ammonia are closer to the results of hydrogen analysis. From an expansion of 50:1 to 100:1 there is less than a two percent increase in the I_{SP} level.
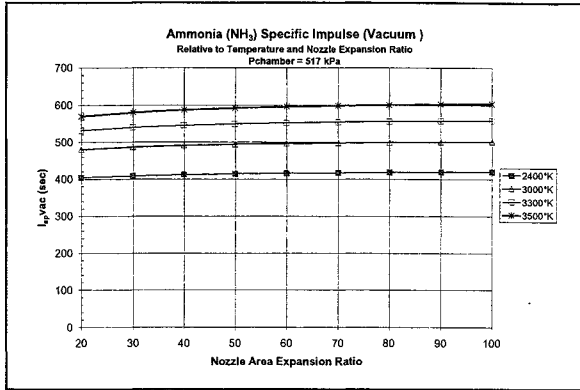
Figure 8. Ammonia I_{SP} at 517 kPa Initial Pressure
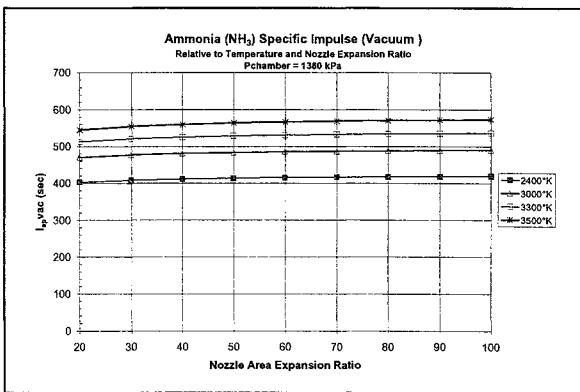
Figure 9. Ammonia I_{SP} at 1380 kPa Initial

The results of this analysis indicate there is an advantage of using lower pressures at higher temperatures to increase the dissociation and thus producing higher I_{SP} values. Further analysis of each propellant at temperatures from 2400 K and higher was made to determine the maximum I_{SP} using a minimum pressure of 69 kPa (10 psia). The pressure was adjusted if necessary to reach the temperature. This data is shown in Table 1 with the I_{SP} values at 517 kPa for comparison. The results show that higher values of I_{SP} are possible but not always at a lower pressure as the methane results indicate. The ideal pressure for the expected temperature of operation is a parameter in the design that would benefit from an optimization exercise for each propellant considered.

Table 1 Maximum I_{SP} Values at 100:1 (Minimum pressure = 69 kPa, expansion ratio = 100:1)

	Pressure	Temperature (K)			
		2400	3000	3300	3500
H_2	517	860	1037	1166	1267
	69	875	1144	1336	1369[†]
CH_4	517	480	588	667	705[††]
	69	485	628	698[†]	705[††]
NH_3	517	421	502	559	604
	69	427	547	634	639[†††]

[†]   Pressure = 165 kPa
[††] Pressure = 910 kPa
[†††] Pressure = 221 kPa

In summary, the baseline propellant hydrogen shows the most promise for obtaining the maximum I_{SP} level. The results indicate a nozzle expansion ratio of 100:1 also maximizes the I_{SP}, however a ratio of 50:1 is probably adequate and helps minimize the weight. A final design process would optimize the expansion ratio with the I_{SP}.

As stated earlier, the ΔV is also a function of the mass ratio or mass fraction. The relationship is logarithmic and basically requires the minimum mass ratio possible. In other words, maximize the throw weight (fuel) and minimize the dry mass (tank structure, probe, nozzle, etc.). The effect of mass ratio relative to ΔV for various I_{SP} values can be represented graphically as shown in Figure 10. This shows that as the mass ratio is decreased to less than 0.5, the increase in ΔV is dramatic.
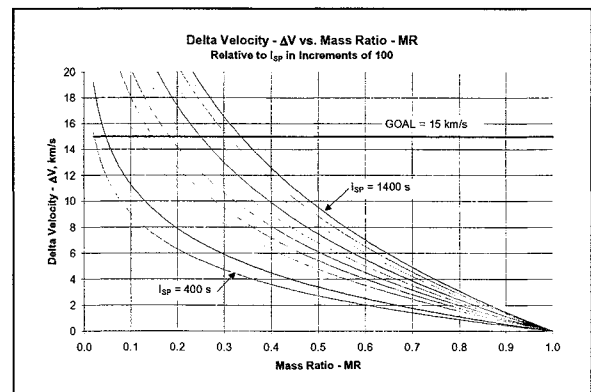
Figure 10. Delta Velocity-ΔV and Mass Ratio-MR

The results of this analysis indicate that in order to meet the ΔV goal of 15 km-s^{-1}, mass ratios of 0.022, 0.078, 0.148, 0.217, 0.280 and 0.335 are needed for I_{SP} values of 400 sec, 600 sec, 800 sec, 1000 sec, 1200 sec and 1400 sec, respectively. A system with a mass ratio close to 0.1 is not uncommon with solid propellant propulsion systems

4

but is difficult to achieve with the liquid or gas propellants. For a deep-space mission with a space-storable bipropellant system, current technology ($N_2O_2+N_2H_2$) yields 317 sec I_{SP} at $\zeta \sim 0.55$.[15]

Preliminary estimates of masses of the main components of the system were made to determine an approximate ΔV and the corresponding V_{ESC} values. The baseline fuel of H_2 is used in the estimates. Table 2 summarizes the weights and includes the mass ratio and mass fraction.

Table 2. Mass Estimate Summary

Probe	50 kg
Thermal Shield	141 kg
LH$_2$ Tank	300 kg
LH$_2$	209 kg
Nozzle & Plenum	50 kg
Total	750 kg
Dry Mass	541 kg
Fuel Mass	209 kg
Mass Ratio	0.721
Mass Fraction	0.279

Based on these estimates the ΔV goal of 15 km-s^{-1} is not achieved. The ΔVs using these estimates are 2.8 km-s^{-1}, 3.3 km-s^{-1}, 3.7 km-s^{-1} and 4.1 km-s^{-1} for the maximum predicted I_{SP} values of 877, 1037, 1166 sec and 1267 sec, respectively. These correspond to V_{ESC} values of 8.7 AU-yr^{-1}, 9.6 AU-yr^{-1}, 10.1 AU-yr^{-1} and 10.6 AU-yr^{-1} from a 4 R_S perihelion. A 3 R_S perihelion increases these values by 7.5% assuming the masses are held constant.

Assuming the volume of the system is the only constraint, the other propellant candidates with lower I_{SP} values could improve the ΔV due to the large decrease in mass ratio. This is due to the combination of density and I_{SP} characteristics of the propellant. For example, by replacing the LH$_2$ (70 kg-m^{-3}) with NH$_3$ (682 kg-m^{-3}) the mass ratio would be decreased to 0.21 and although the maximum predicted I_{SP} values of 421 sec, 502 sec, 559 sec and 604 sec are lower than those for H$_2$, the resultant ΔVs are 6.4 km-s^{-1}, 7.7 km-s^{-1}, 8.6 km-s^{-1} and 9.3 km-s^{-1}. This increase in ΔV values of approximately 230% increases the V_{ESC} values 52% to 13.3 AU-yr^{-1}, 14.5 AU-yr^{-1}, 15.3 AU-yr^{-1} and 15.9 AU-yr^{-1} from a 4 R_S perihelion. The disadvantage to this is that the total weight of the system increases to 2577 kg.

Whether the high specific impulse propellant (H$_2$) or the high-density propellant (NH$_3$) is used, the next hurdle is to optimize the system for a minimum dry mass and maximum propellant mass while maintaining structural and thermal integrity.

The propellant management system (nozzle, heat exchanger, etc.) would be optimized to provide the thrust for the necessary action time. This effort may be necessary in determining the best propellant.

THERMAL ANALYSIS

The propellant for the system is stored until needed for the ΔV maneuver at perihelion. At this time, heating is required to produce the necessary I_{SP}. The solar propulsion concept utilizes the Sun as the energy source to accomplish this task. For this system, the panels used for the exterior heat shields (see Figure 2) were identified as the most practical heat exchanger system. In order to minimize complexity and weight, the goal was to use only the center heat shield panel. The entire exterior heat shield is a 5-meter long carbon-carbon cylinder with a 1.37-meter radius, providing a surface area of 43.1 m^2. The heat shield is divided into three sections of 120 degrees, each with surface areas of 14.3 m^2 that fold out to provide protection for the interior components of the system.

The heat-exchanger concept uses carbon-carbon channels that run parallel to the axis of the heat shield cylinder, as shown in Figure 3, as the heat exchanger "core". Inlet and outlet headers, not shown in the figure, would connect the flow to the supply tank and the nozzle. A parametric thermal analysis was performed to determine the effect of the various design parameters on the H$_2$ propellant (a thermal analysis for NH$_3$ and CH$_4$ is not included in this study). The spacing of the channels was one of the variables in the parametric analysis, along with the number of plies for the carbon-carbon material (this effected the "fin efficiencies" of the internal heat transfer surfaces). Flow rate and incident heat flux are also included in the parametric study.

The heat exchanger was modeled using a finite-difference scheme with 1000 differential sections along the 5-meter length. For each section, the local temperature and pressure were calculated based on incident heat flux, inlet gas temperature and inlet gas pressure. For this analysis, surface reradiation, conductive wall resistance, and surface efficiencies were considered. Radiative losses at the back wall (interior surface of the heat shield) are based on the (higher) surface temperature of the front surface (exterior surface of the heat shield) for a conservative estimate. Nusselt numbers and friction factors were calculated using standard correlations based on local Reynolds number (laminar/turbulent). Flow development effects were was not considered due to the long channel length as compared to the effective channel diameter.

The H$_2$ thermal properties required for the analysis are based on handbook values for

temperatures up to 200 K, with extrapolation for higher temperatures. The carbon-carbon thermal conductivity is based on a linear fit for known values of 286 W/m-K at 300 K and 67 W/m-K at 2400 K. Emissivity (ε) for the carbon-carbon material is assumed to be 0.9 for the initial analysis. The incident heat flux is initially assumed to be a conservative 381 W-cm^{-2} at 4 R_S. An average value for the incident heat flux would be 401 W-cm^{-2} at 4 R_S and 713 W-cm^{-2} at 3 R_S using a solar luminosity of 9.33e25 cal/sec and R_S of 6.96e10 cm.[16] The analysis is also based on the assumption that the incident heat flux is completely absorbed by the heat shield.

The maximum possible surface temperature, T_s, of the heat shield occurs when reradiation, including the back wall radiation loss, equals the incident radiation. That is, the maximum temperature occurs when the net surface heat flux is zero, as shown in the equation

$$\dot{Q} = \dot{Q}_{inc} - 2\varepsilon\sigma A_s T_s^{4} = 0$$

where σ is the Stefan-Boltzmann constant, and the factor of 2 conservatively accounts for emission from the back surface at the same temperature as the front. The fluid temperature cannot exceed this maximum surface temperature. For an incident heat flux of 381 W-cm^{-2} and an emissivity of 0.9, the maximum temperature is 2472 K, as compared to 2504 K if the average incident heat flux of 401 W-cm^{-2} is used. However, this would increase to 2891 at 3 R_S, for which the nominal incident heat flux is 713 W-cm^{-2}. Use of a surface material with a lower emissivity has the most potential for increasing the maximum temperature. For example, a material with an emissivity of 0.3 (at the longer wavelengths associated with reradiation) increases the maximum temperature to 3295 K and 3805 K at 4 R_S and 3 R_S, respectively.

A set of parameters and values for the parametric analysis were defined as follows:

Incident heat flux:	381 W-cm^{-2}
# of plies (thickness):	1 (0.3 mm)
	2 (0.6 mm)
	3 (0.9 mm)
Channel size:	5 mm
	10 mm
	15 mm
Mass flow rate:	200 g/s
	1100 g/s
	2000 g/s

The incident heat flux of 381 W-cm^{-2} is selected to evaluate the minimum expected heat transfer capability. Results from the structural

analysis, discussed below, shows that one-ply of carbon-carbon is not feasible and two-ply is marginal. However, one test case using one-ply of carbon-carbon is analyzed. A set of mass flow rates from a minimum desired rate of 200 g/s to a high rate of 2000 g/s is used to bound the possible range. Based on these preliminary findings and assumptions, the matrix shown in Table 3 was made for the parametric study. Inlet pressures were determined such that the final pressure is at least 350 kPa (50 psi).

Table 3. Parametric Analysis Matrix

Test Case	Q_{inc} W/cm^2	# of plies	Channel Size mm	Flow Rate g/s	Pinlet KPa
1	381	1	10	200	500
2	381	3	5	200	500
3	381	3	10	200	500
4	381	3	15	200	500
5	381	3	5	1100	1500
6	381	3	10	1100	500
7	381	3	15	1100	500
8	381	3	5	2000	1800
9	381	3	10	2000	1800
10	381	3	15	2000	1800

The results of this analysis indicate that the flows above 1100 g/s were too high to allow the fluid temperature to reach the maximum surface temperature. Channel size affected both the pressure drop and the asymptotic temperature. The pressure drop is greatest with the 5 mm channel while there is the least degradation of asymptotic temperature for the same channel size. Results of the test cases 2 thru 4 are shown in Figures 11, 12 and 13. The maximum predicted temperatures achieved with test cases 2, 3, and 4 are 2471 K, 2448 K, and 2368 K, respectively. The corresponding pressure drops are 90 kPa, 7 kPa, and 2 kPa.
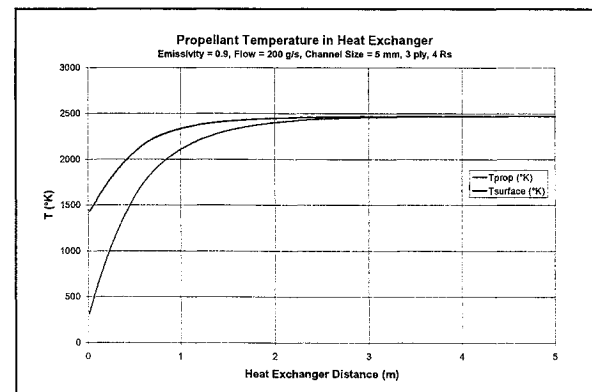
Figure 11. Parametric Analysis – Test Case 2

6
American Institute of Aeronautics and Astronautics

Based on these results, the recommended channel size is 10mm. At this channel size, the propellant temperature is within one percent of the surface temperature and the pressure drop is minimal. The actual size could be optimized and would probably be less than 10 mm. Further analysis was performed to narrow the range in flow rate capability since the range between the low and middle values originally selected was so large. This analysis shows that flow rates higher than 500 g/s result in excessive degradation of the asymptotic temperature and are not desirable for the 10 mm channel size.
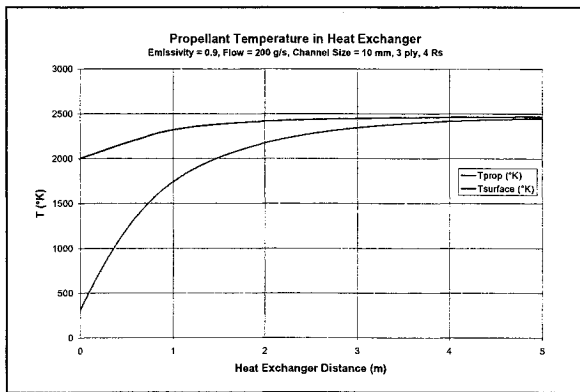
Figure 12. Parametric Analysis – Test Case 3
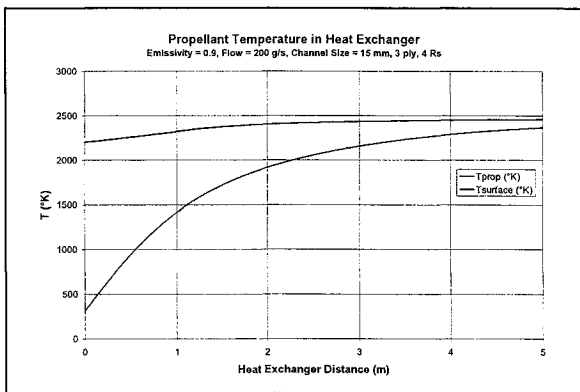
Figure 13. Parametric Analysis – Test Case 4

The possibility of increasing the asymptotic temperature by decreasing the emissivity was also investigated. One proposed method for reducing the emissivity is to apply a thin (~15μ) coating of tungsten on the heat exchanger. This concept was analyzed for the configuration with 10 mm channels, 3-ply carbon-carbon material and a flow rate of 232 g/s. An emissivity of 0.3 was the lowest value analyzed and the corresponding results are shown in Figure 14. This increases the outlet temperature to 3200 K. An additional increase in asymptotic temperature is achievable with an increase in incident

heat flux. This is accomplished with a ΔV maneuver at a perihelion of 3 R_S where the incident heat flux is increased to 713 W-cm^{-2}. In order to prevent the maximum temperature of the carbon-carbon material from exceeding 3500 K, the emissivity of the heat shield needs to be a value of 0.4 or higher. The results of analyzing with these parameters are shown in Figure 15.

STRUCTURAL ANALYSIS

The structural analysis was performed to evaluate the heat exchanger concept of the propulsion system. The heat exchanger is assumed to consist of the heat shield center panel only. The heat shield is carbon-carbon with channels that run the full length. The channel sizes were varied along with the material thickness or number of plies for this analysis. A typical configuration of the channeled heat exchanger is shown in Figure 3.
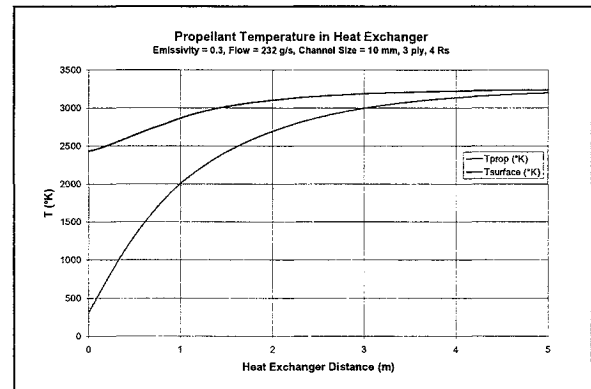
Figure 14 Thermal Analysis – Emissivity = 0.3
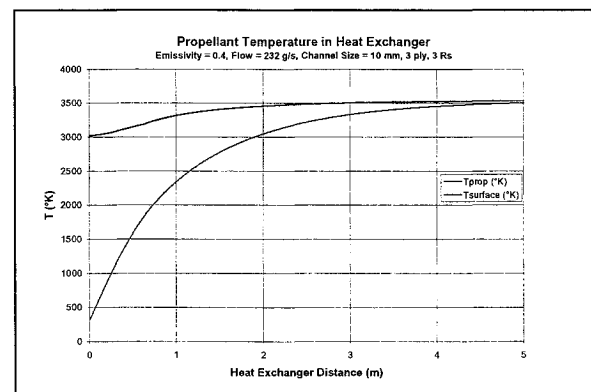
Figure 15 Thermal Analysis – 3 Rs

The channel sizes that were considered include 5 mm and 10 mm. The thickness of the material was varied from 1 to 6 plies in increments of 1 ply where each ply was 0.3 mm thick. The typical carbon-carbon material properties at 3000°F (1922 K) were used in this analysis. The pressure level

7

American Institute of Aeronautics and Astronautics

assumed for the evaluation is 200 psi (1379 kPa), which makes the analysis more conservative if 75 psi (517 kPa) is the best pressure for the desired I_{SP}. The acceptable configurations were determined using stress criteria. The results of this analysis are shown in Table 3.

Table 3. Heat Shield Maximum Stress, psi

# of Plies	Channel Size	
	5 mm	10 mm
1 ply (0.3 mm)	**23,740**	**91,890**
2 ply (0.6 mm)	4,278	**22,450**
3 ply (0.9 mm)	1,996	6,571
4 ply (1.2 mm)	1,249	4,044
5 ply (1.5 mm)	874	2,779
6 ply (1.8 mm)	658	1,930

*Allowable stress ~ 14,000 psi

This analysis shows that for both sizes of channels the 1-ply design is unacceptable. The 2-ply design is acceptable for the 5 mm size only, while the remaining designs are acceptable for both channel sizes.

CONCLUSIONS

The overall goal is to achieve a 20 AU-yr^{-1} (94.8 km-s^{-1}) escape velocity from the solar system, which requires a ~15 km-s^{-1} ΔV maneuver at perihelion using the STP system. An initial assessment suggested this to be a possibility if the propulsion system could deliver an I_{SP} of 1000+ sec. The STP system can deliver an I_{SP} in that range based on the assumptions made in this report.

However, there is more required to achieve the overall goal. The next big driver after the I_{SP} of the system is the mass ratio. To obtain the mass ratio values discussed, while using a low molecular weight propellant, requires the optimization of structural masses and an innovative way to carry and store the propellant for the long period of time before actually requiring its use. Since the tank is the heaviest major component of the system, its optimization is the highest priority. The heat shield (and heat exchanger) is the next component in priority order for optimization for mass reduction. The design described in this report is very preliminary and has room for such optimizations.

The heat exchanger/heat shield described in the report can serve both purposes but to achieve the higher I_{SP} values the temperature must be higher than the baseline case. One of the means of achieving such a higher temperature is to lower the emissivity from that of carbon-carbon by using a coating of low emissive material such as tungsten. Processes similar to this have been done in the past but would still need to be evaluated and demonstrated for this specific

requirement. An additional complication is the relatively large size of the heat exchanger and the relatively large mismatch of the coefficients of thermal expansion for carbon-carbon and tungsten.

A second method of achieving the higher temperatures after reducing the emissivity, is through increasing the incident heat flux. This is possible with a ΔV maneuver at a perihelion of 3 R_S. This not only increases the maximum possible propellant temperature but also decreases the required ΔV. Any optimization in this area would need to consider the mass change in the heat shield and its affect on the mass ratio since closer maneuvers probably require more shielding.

REFERENCES

1. Jaffe, L. D. and C. V. Ivie, Science aspects of a mission beyond the planets, *Icarus, 39*, 486-494, 1979.
2. Holzer, T. E., et al. The Interstellar Probe: Scientific objectives for a Frontier mission to the heliospheric boundary and interstellar space, NASA Publication, 1990.
3. Mewaldt, R. A., J. Kangas, S. J. Kerridge, and M. Neugebauer, A small interstellar probe to the heliospheric boundary and interstellar space, *Acta Astron., 35*, Suppl., 267-276, 1995.
4. McNutt, R. L., Jr., R. E. Gold, E. C. Roelof, L. J. Zanetti, E. L. Reynolds, R. W. Farquhar, D. A. Gurnett, and W. S. Kurth, A sole/ad astra: From the Sun to the stars, *J. Brit. Inter. Soc., 50*, 463-474, 1997.
5. McNutt, R. L., Jr., G. B. Andrews, J. McAdams, R. E. Gold, A. Santo, D. Oursler, K. Heeres, M. Fraeman, and B. Williams, A realistic interstellar explorer, *STAIF-2000 Proc.*, 2000.
6. Liewer, P. C., R. A. Mewaldt, J. A. Ayon, and R. A. Wallace, NASA's interstellar probe mission, *STAIF-2000 Proc.*, 2000.
7. McNutt, R.L., *A Realistic Interstellar Explorer*, Phase I Final Report, NASA Institute for Advanced Concepts, NIAC CP98-01, May 1999.
8. R. L. McNutt, Jr., G. B. Andrews, J. McAdams, R. E. Gold, A. Santo, D. Oursler, K. Heeres, M. Fraeman, and B. Williams, Low-Cost Interstellar Probe, paper IAA-L-0608, Fourth IAA

International Conference on Low-Cost Planetary Missions, Acta Astronautica, in press 2001.

9.   R. L. McNutt, Jr., G. B. Andrews, J. V. McAdams, R. E. Gold, A. G. Santo, Douglas A. Ousler, K. J. Heeres, M. E. Fraeman, and B. D. Williams, A Realistic Interstellar Probe, Proceedings, COSPAR Colloquium on The Outer Heliosphere: New Frontiers, Potsdam, Germany, July 24-28, 2000, in press 2001.

10. Ehricke, K. A., The solar-powered spaceship, *American Rocket Society Paper 310-56*, June 1956.

11. Ehricke, K. A., 21.3 Solar propulsion, in *Handbook of Astronautical Engineering*, H. H. Koelle, ed., McGraw-Hill Book Company, Inc., New York, 1961.

12. Laug, K. *The Solar Propulsion Concept is Alive and Well at the Astronautics Laboratory*, AFRL, Edwards Air Force Base CA, JANNAF Propulsion Meeting, Cleveland OH, May 1989.

13. Kennedy F., Jacox M., *Mission Applications of an Integrated Solar Upperstage (ISUS)*, ASME paper AP0401, 1995.

14. Ehricke, K. A., Saturn-Jupiter rebound, *J. Brit. Int. Soc., 25*, 561-571, 1972.

15. Santo, A. G., R. E. Gold, R. L. McNutt, Jr., S C. Solomon, C. J. Ercol, R.W. Farquhar, T. J. Hartka, J. E. Jenkins, J. V. McAdams, L. E. Mosher, D. F. Persons, D. A. Artis, R. S. Bokulic, R. F. Conde, G. Dakermanji, M. E. Goss, Jr,, D. R. Haley, K. J. Heeres, R. H. Maurer, R. C. Moore, E. H. Rodberg, T. G. Stern, S. R. Wiley, B. G. Williams, C.-L. Yen, and M. R. Peterson, The MESSENGER Mission to Mercury: Spacecraft and mission design, *Planetary and Space Science, Special Issue,* accepted 2001.

16. Kreith, F., "Radiation Heat Transfer for Spacecraft and Solar Power Plant Design," International Textbook Co., 1962.